
Final Technical Report for:

***MULTI-DIMENSIONAL MODELING OF PRESSURIZATION AND EXPULSION
OF MULTI-PHASE HYDROGEN PROPELLANT***

NASA Grant NAG3-1292

Period of Performance: August 1991 - July 1993

Principal Investigator: Professor John I. Hochstein
Memphis State University
Memphis, TN 38152

The two AIAA papers contained within this document present the research and results produced through the support provided by NASA Grant NAG3-1292: *Multi-Dimensional Modeling of Pressurization and Expulsion of Multi-Phase Hydrogen Propellant*.



AIAA 91-2407

**Computational Modeling of the
Pressurization Process in a NASP
Vehicle Propellant Tank Experimental
Simulation**

G.P. Sasmal, J.I. Hochstein, M.C. Wendl
Washington University,
St. Louis, Missouri

and

T.L. Hardy
NASA Lewis Research Center
Cleveland, Ohio

**AIAA/SAE/ASME/ASEE
27th Joint Propulsion Conference
June 24-26, 1991 / Sacramento, CA**

COMPUTATIONAL MODELING OF THE PRESSURIZATION PROCESS IN A NASP VEHICLE PROPELLANT TANK EXPERIMENTAL SIMULATION

G. P. Sasnal*, J. I. Hochstein**, M. C. Wendl*
Washington University, St. Louis, Missouri 63130

T. L. Hardy+
NASA Lewis Research Center, Cleveland, Ohio 44135

ABSTRACT

A multidimensional computational model of the pressurization process in a slush hydrogen propellant storage tank was developed and its accuracy evaluated by comparison to experimental data measured for a 5 ft diameter spherical tank. The fluid mechanic, thermodynamic, and heat transfer processes within the ullage are represented by a finite-volume model. The heat and mass fluxes at the ullage boundary were computed in auxiliary analyses and specified as input to the finite-volume model. The model was shown to be in reasonable agreement with the experiment data. A parameter study was undertaken to examine the dependence of the pressurization process on initial ullage temperature distribution and pressurant mass flow rate. It is shown that for a given heat flux rate at the ullage boundary, the pressurization process is nearly independent of initial temperature distribution. The mass flow rate study revealed decreasing pressurant mass requirement with increasing pressurant mass flow rate. Further, significant differences were identified between the ullage temperature and velocity fields predicted for pressurization of slush and those predicted for pressurization of liquid hydrogen. A simplified model of the pressurization process was constructed in search of a dimensionless characterization of the pressurization process. It is shown that the relationship derived from this simplified model collapses all of the pressure history

data generated during this study into a single curve.

Nomenclature

c_v	Specific heat at constant volume
h_g	Specific enthalpy of pressurant gas
\dot{m}_g	Pressurant mass flow rate
p	Tank pressure
$Q_{l/s}$	Heat transfer rate to liquid/slush H_2
Q_w	Rate of heat transfer to the tank wall
R	Gas constant
t	Time
t_p	Total pressurization time
T	Temperature
V	Tank ullage volume
ρ	Density of the gas in the tank

Subscripts

f	Final state
i	Initial state

INTRODUCTION

Vehicles which use cryogenic propellants because of their high specific impulse, incur the difficulties associated with managing the propellant prior to its use. The propellant management issue of interest in this study is the pressurization of a vehicle propellant storage tank prior to engine ignition. This pressurization may be required to alleviate feed-line cavitation problems or may provide the sole motive force for transporting propellant from the storage tank to the

* Research Associate, Member AIAA

** Associate Professor, Associate Fellow AIAA

+ Aerospace Engineer, Member AIAA

engine. Since all methods proposed for tank pressurization require on-board resources (such as pressurant gas), optimization of the pressurization process is important for efficient vehicle design and operation. Optimization requires an understanding of the complex fluid dynamic and thermodynamic processes occurring in cryogenic propellant management systems and research into these processes has been pursued for over 20 years^{1,2,3}.

The proposal to use a mixture of solid and liquid hydrogen (known as slush hydrogen) as the storage medium for the National Aerospace Plane (NASP) presents a formidable challenge to understanding the pressurization process in the propellant storage tanks for such a vehicle. Modeling the pressurization process requires simultaneous solution of fluid mechanic, thermodynamic, and heat transfer models for a tank in which three phases of matter are present. Most existing models^{1,4} are fundamentally one-dimensional and based on simplifying assumptions and experimentally derived correlations. Although these models have served well in the past, their range of validity is limited by the range of cases from which they are derived. It is not clear that they are adequate as design tools for future vehicle development. Since the flow field and temperature field in a tank during pressurization are in actuality multi-dimensional, it is reasonable to expect that accurate modeling of the pressurization process will require inclusion of the multi-dimensional effects. One study⁵, using the same computational technology as the present study, has been performed to examine certain multidimensional effects. The current study was undertaken to identify or develop a tool for multi-dimensional modeling of the pressurization process and to use that tool to begin a study of the parametric dependence of the pressurization process.

The first phase of this study identified the FLOW-3D code⁶ as a good candidate for modeling the pressurization process and demonstrated its accuracy by comparing computational predictions to experimental data. The second phase was a study of the parametric dependence of the pressurization

process on initial ullage temperature distribution and pressurant mass flow rate. The third phase was development of a dimensionless characterization of pressurization by construction of a simplified model and examination of the physical processes which occur in the ullage during pressurization. The sections of this paper are organized to reflect this sequence of efforts. The final section summarizes the results of the entire study and presents conclusions drawn from these results.

EXPERIMENT CONFIGURATION

The experiment configuration modeled during this study was a 5 ft diameter spherical tank partially filled with liquid/slush hydrogen. The tank was pressurized by injecting gaseous hydrogen through a 1 ft diameter hemispherical diffuser located at the top of the tank. The pressurization process was initiated at the appropriate saturation pressure, (1.1 psia for slush hydrogen or 17.4 psia for liquid hydrogen), and was terminated when the tank internal pressure reached 50 psi. Although the experimental procedure then proceeded to a hold period followed by expulsion of the propellant, the focus of this study is on the pressurization process. A schematic of the tank configuration is shown in Fig. 1. A typical tank pressure history recorded during the pressurization of liquid hydrogen is shown in Fig. 2.

EVALUATION OF THE COMPUTATIONAL MODEL

The first phase of the study required identification or development of a computational tool capable of modeling the pressurization process. At a minimum, this requires the ability to model the transient low-speed compressible flow of an ideal gas, including heat transfer effects, in a reasonable representation of the geometry of interest. An important secondary consideration was the ability of the tool to also model the expulsion process. Since the fluid level in the tank changes during the expulsion process, this requires modeling the flow of an incompressible fluid with a vapor/liquid interface that changes position with time. The FLOW-3D

code⁶ was selected as the highest rated candidate because it appeared to meet all of the basic requirements and because of previous successful applications to similar problems^{5,8}.

FLOW-3D is designed to model transient flows of fluid and thermal energy in three space dimensions in complicated geometries which may include free surfaces. Either Cartesian or cylindrical coordinates may be used to define the problem geometry and two-fluid calculations can be performed. Some of the models and features which contributed to selecting FLOW-3D for this study include: a compressible flow model (ideal gas), a two-fluid interface model, time-dependent boundary conditions, a thermal buoyancy model, a surface tension model, and a turbulent flow model. To efficiently use the available computational resources, the code is divided into a pre-processor, a main-processor, and a post-processor. The pre-processor resides on a VAX and is the interface through which the problem was defined. The data is then transferred to a Cray XMP where the main processor performs the analysis and generates the output files which are returned to the VAX for post-processing. A typical run for this study, using a two-dimensional pie-sector model of the tank, required approximately 25 minutes of CPU time on the Cray.

The first step in the evaluation process was to determine a suitable computational model for the spherical tank. Experimental data¹ obtained for pressurization of a tank with 56% ullage by volume was selected to test the performance of FLOW-3D. The free surface of the liquid hydrogen was modeled as a solid boundary to eliminate the need for a two-fluid model. Evaporation/condensation at the liquid free surface was neglected. Since detailed measurements of the pressurant gas flow rate were not obtained during preliminary analyses that the flow rate was a constant value computed by dividing the total mass added during the run by the pressurization time. Heat transfer rates to the tank wall and to the liquid/slush were taken from SLURP code analyses⁴, ($\dot{Q}_w=5.02$ Btu/sec, $\dot{Q}_{l/s}=0.46$ Btu/sec). The

diffuser at the pressurant gas inlet was modeled as a porous media.

Since all of the planned analyses were defined by axisymmetric boundary conditions for axisymmetric geometries, the first goal was to establish the validity of replacing a true three-dimensional model, (radial, azimuthal, axial), with a pie-sector model, (radial, θ , axial), to reduce the computational demands for completing the study. The first configuration under examination was analyzed using a pie-sector model (10x1x10) and a fully three-dimensional model (10x36x10). Comparing the predicted velocity and temperature fields at a slice through a diameter of the fully three-dimensional model to those predicted by the pie-sector model revealed nearly identical solutions. To establish confidence that the pie-sector mesh was sufficiently refined, a convergence study was performed using a 15x1x15 mesh and a 10x1x20 mesh. Although the finer meshes revealed some details missing from the first mesh, the predicted fields for the finer meshes did not qualitatively differ from those predicted by the first mesh. Since the liquid free surface was modeled as a solid boundary with a specified heat flux, the improved temperature gradient near the free-surface predicted using the finer meshes is not a significant factor for these analyses, but could become significant for analyses in which heat and mass transfer at the free surface is computed. It was therefore concluded that a 10x1x10 pie-sector mesh would be used for all subsequent analyses in this study.

The second step in the evaluation process was to compare computational predictions to experimentally obtained data. Since the pressurant inlet pressure was not measured during the experiment, a value of 50 psi was assumed for the inlet pressure based on other known parameters in the experiment. The pressurant inlet mass flow rate is a key parameter which must be specified to the computational model but which was not recorded during the experiment. The S-curve of the pressure history displayed in Fig. 2 suggests that, contrary to initial assumptions, the flow rate during the experiment was a function of time. A sequence of

analyses were performed during which the flow rate history was iteratively adjusted until the pressure history predicted by FLOW-3D matched the history displayed in Fig 2.

The difference between measured and computationally predicted total mass added was less than 15%. Although this difference is larger than had been hoped for, several factors contributed to this difference. As detailed above, important input parameters, such as pressurant inlet pressure and flow rate history, were estimated or back-calculated because they had not been measured during the experimental effort. Given the level of uncertainty in the problem definition, the agreement between experimental and computational results was considered adequate to proceed with the investigation. To eliminate this uncertainty in future efforts, a list of recommended measurements for future experimental studies is provided in the concluding remarks of this paper.

PARAMETRIC STUDY OF PRESSURIZATION PROCESS

Table 1 presents a summary of the input parameters and the performance predictions for the twelve cases studied during this effort. An initial pressure of 17.4 psi indicates pressurization of liquid hydrogen whereas an initial pressure of 1.1 psia indicates that slush hydrogen was pressurized. For all analyses, the pressurant gas inlet pressure was specified to be 50 psi, the inlet temperature to be 307 °R, and the heat flux rates were specified to be $Q_w=5.02$ Btu/sec and $Q_{l/s}=0.46$ Btu/sec. The pressurant mass flow rate for each case was assigned a constant value which is listed in Table 1. The analysis matrix defined in Table 1 represents studies of different parametric effects which are described in detail in the balance of this section.

The first study focused on the influence of initial temperature distribution within the ullage on the pressurization process. The ullage temperature distribution had not been measured during the experimental investigation so two bounding cases

Table 1 Analysis Matrix (55.6% ullage)

Case #	*Initial Pressure (psia)	*Initial Temp. (°R)	*Inlet Velocity (ft/s)	**Press. Time (s)	**Mass Added (lb _m)	**Flow Rate (lb _m /s)	**Final Pressure (psia)
1	17.4	60-40	1.393	33.0	0.771	0.0234	50.2
2	1.1	60-40	1.393	54.0	1.262	0.0234	49.8
3	17.4	250-40	1.655	26.0	0.720	0.0277	49.8
4	17.4	60-40	1.655	26.0	0.720	0.0277	49.8
5	1.1	60-40	1.655	43.0	1.193	0.0277	50.4
6	1.1	250-40	1.655	43.0	1.193	0.0277	50.4
7	17.4	60-40	2.500	15.5	0.649	0.0419	49.5
8	1.1	60-40	2.500	25.5	1.070	0.0419	50.1
9	17.4	60-40	3.500	10.5	0.612	0.0583	49.3
10	1.1	60-40	3.500	17.0	0.992	0.0583	49.2
11	17.4	60-40	5.000	7.2	0.600	0.0832	49.7
12	1.1	60-40	5.000	11.5	0.958	0.0832	49.3

* specified value

** computationally predicted value

were selected: the 60-40 °R distribution was selected to represent a fairly well mixed ullage whereas the 250-40 °R distribution was selected to represent a thermally stratified ullage. The temperature fields predicted at the end of the pressurization process for both temperature distributions and for both propellants (cases 3, 4, 5, 6) are displayed in Fig. 3. Review of Table 1 reveals that, given the same heat flux rate at the tank wall, the pressurization time appears to be independent of initial ullage temperature distribution. Although the global pressurization performance as measured by total mass added and pressurization time is unchanged by the different initial ullage temperature distributions, the detailed temperature profiles do show some differences. In particular, the clustering of temperature contours at the surface of the slush hydrogen (for the low initial pressure) indicates that there may be a significant difference in heat transfer and mass transfer rates at the slush/vapor interface than at the liquid/vapor interface. Since the current model uses a specified heat transfer rate at the free surface, and assumes zero mass transfer at the free surface, this hypothesis is unprovable with the present modeling capability and remains a topic for future study.

The relationship between pressurization time and pressurant flow rate revealed by the matrix of cases in Table 1 is displayed in Fig. 4. Although the decrease in pressurization time with increasing mass flow rate is expected, it should be noted that the relationship is not a simple inverse proportionality. Figures 5 and 6 present one of the most interesting results of the study. The computationally predicted relationship between pressurization time and the total pressurant mass addition required to pressurize the tank to 50 psi is displayed in Fig. 5. The relationship between pressurant mass flow rate and the total mass addition required is displayed in Figure 6. The two relationships are consistent and lead to the conclusion that a more rapid pressurization requires less pressurant mass than a slow pressurization. Although this conclusion may be counterintuitive, the explanation lies in the imposed thermal boundary conditions. A longer pressurization time, coupled with

the constant heat flux specified at the tank walls and at the liquid/slush interface, results in a greater cooling of the ullage. At the lower vapor temperature, a greater vapor mass is required to reach the desired pressure level. Review of the SLURP study report⁴ reveals data to support this conclusion and a comment on this trend by those researchers. Therefore, the ability of the FLOW-3D model to correctly predict this trend lends additional confidence to the validity of the computational model, and brings additional attention to this interesting and potentially important phenomena.

The dependence of velocity and temperature fields in the ullage at the end of pressurization on the pressurant mass flow rate was examined by extracting appropriate data from the results generated by the analysis matrix defined in Table 1. All the analyses examined for this study began with the 60-40 °R ullage temperature distribution and proceeded from an initial saturation pressure to a final pressure of 50 psi. Figure 7 presents computed velocity fields in the ullage for pressurization of liquid hydrogen and Fig. 8 presents the corresponding temperature fields. For the range of inlet mass flow rates examined, the entering gas jet never fully penetrated into the ullage volume. As the flow rate increases a vortex is established at the top of the tank near the inlet diffuser. The temperature near the free surface varies from 50.5 °R to 57.4 °R for the range of pressurant mass flow rates studied. Although the presence of the jet is apparent in the temperature contours, the bulk of the ullage space is well represented by an axial temperature distribution with little radial dependence.

The velocity fields computed for pressurization of slush hydrogen are presented in Fig. 9 and the corresponding temperature fields in Fig. 10. Comparing Fig. 9 to Fig. 7 reveals that substantially different flow patterns are established during slush pressurization than during liquid pressurization. At the lower flow rates, the incoming jet again fails to fully penetrate the ullage and establishes a vortical flow near the inlet. At the higher flow rates, the incoming pressurant jet is seen to fully penetrate the ullage

volume and to establish a variety of flow patterns. At an intermediate flow rate, the jet penetrates all the way to the slush surface and then follows a serpentine path establishing two side-by-side vortices. At the highest flow rate, the jet penetrates to the slush surface and moves radially outward along the surface toward the tank wall. Although two vortices are again formed, they are arranged one-above-the-other instead of side-by-side. Examining Fig. 10 shows that the variety of flow patterns predicted for slush pressurization is reflected in the variety of ullage temperature distributions. At the higher flow rates, the uniformity of temperature with radial location observed for liquid pressurization is replaced with highly radially dependent temperature distributions. The predicted ullage temperature near the slush surface increases from 169 °R for the lowest inlet mass flow rate to 286 °R for the highest flow rate, as compared to approximately 60 °R for the liquid cases.

Comparing the predicted temperature and velocity fields for pressurization of liquid hydrogen to those predicted for slush hydrogen revealed some significant differences. These differences in turn raise concern about some of the modeling assumptions used to perform the analyses. The highly stratified ullage temperature distributions produced by pressurization of liquid hydrogen lead to relatively low gas temperatures near the liquid/vapor interface which, when coupled with the nearly stagnant state of gas near the free surface, seem to support the modeling assumption of constant heat flux with negligible mass transport at the liquid/vapor interface. In contrast, high gas temperatures predicted during pressurization of the slush, coupled with significant flow velocities predicted near the free surface, lead one to seriously question this modeling assumption. Since evaporation or condensation can have a significant effect on the tank internal pressure, caution should be used in accepting computational predictions which do not include these effects. To definitively resolve this concern requires modeling capabilities beyond the those of the present computational tool.

The evolution of temperature and velocity fields observed during the inlet mass flow rate dependence study naturally lead to a curiosity about the dependence of the tank pressure history on inlet mass flow rate. Figure 11 displays the tank pressure histories predicted for pressurization of liquid hydrogen. The tank pressure histories predicted for pressurization of slush are displayed in Fig. 12. Although the trends are not surprising, it should be noted that the rate-of-change of pressure is not constant during the pressurization process but rather increases slightly with increasing elapsed time. A desire to understand this behavior lead to the modeling and dimensional analysis described in the next section.

A Simplified Model and Non-Dimensional Characterization

If multidimensional effects of the pressurization process are neglected, and the ullage is modeled as a lumped thermodynamic entity, a simplified analytical model of the pressurization process can be readily developed. Conservation of thermal energy can be enforced by satisfying a balance equation written for the ullage volume:

$$c_v \dot{V} \frac{d(\rho T)}{dt} = \dot{m}_g h_g - \dot{Q}_w - \dot{Q}_{l/s} \quad [1]$$

where \dot{Q}_w includes any discrete "heat leaks" into the ullage as well as convective heat transfer from the ullage to the tank wall. The product of density with temperature in the derivative can be replaced by an expression including pressure by assuming that the ullage can be modeled as an ideal gas ($\rho T = p/R$).

$$\frac{dp}{dt} = \frac{R}{c_v \dot{V}} (\dot{m}_g h_g - \dot{Q}_w - \dot{Q}_{l/s}) \quad [2]$$

This form clearly shows that, for constant specified heat flux at the boundaries and constant pressurant mass flow rate, this lumped model predicts a constant rate-of-change of tank internal pressure with time. This is in qualitative agreement with the near-constant pressurization rate predicted

by the computational model. The difference is due to the multidimensional effects incorporated into the computational model which cannot be included in the simple lumped model.

Since one goal of the modeling and analysis is to develop correlating parameters for the pressurization process, it is important to select appropriate normalizing or non-dimensionalizing scales. One logical time scale is the elapsed time required to complete the pressurization process.

$$t^* = \frac{t}{t_f} \quad [3]$$

The total change in pressure to be accomplished by the pressurization process was selected to normalize the pressure rise from pressurization initiation.

$$p^* = \frac{p - p_i}{p_f - p_i} \quad [4]$$

It was hoped that this combination of characteristic scales would produce a nondimensional representation of the pressurization process which would produce a single relationship for all the pressurization cases. Combining the nondimensional variables defined in Eqs. 3 and 4 produces the following expression for the rate-of-change of nondimensional pressure with normalized time.

$$\frac{dp^*}{dt^*} = \frac{d\left(\frac{p - p_i}{p_f - p_i}\right)}{d\left(\frac{t}{t_f}\right)} = \left(\frac{t_f}{p_f - p_i}\right) \frac{dp}{dt} \quad [5]$$

Recalling that dp/dt is constant for constant heat flux and flow rate boundary conditions, integrating this expression over the elapsed time required for pressurization yields the following result.

$$p_f^* - p_i^* = \left(\frac{t_f}{p_f - p_i} \frac{dp}{dt}\right) (t_f^* - t_i^*) \quad [6]$$

Rearranging, and substituting appropriate values into this equation, produces the following result.

$$\left(\frac{t_f}{p_f - p_i}\right) \frac{dp}{dt} = \frac{p_f^* - p_i^*}{t_f^* - t_i^*} = \frac{1 - 0}{1 - 0} = 1 \quad [7]$$

Therefore, for any pressurization analysis with specified constant mass inflow rate and constant heat flux boundary conditions:

$$\frac{dp^*}{dt^*} = 1 \quad [8]$$

Since this result is independent of specific values for any of the parameters required for the computation, the goal of a "universal" relationship for all pressurization processes has been satisfied (for the lumped parameter model).

Since the computational model includes multidimensional effects which cannot be included in the lumped parameter model, the validity of dp^*/dt^* as a correlating parameter for pressurization analyses must be evaluated against the results from the analysis matrix defined in Table 1. The tank pressure history data previously displayed in Figs. 11 and 12 were reorganized using the new dimensionless variables to produce Fig. 13. Careful examination reveals that, although dp^*/dt^* is not precisely equal to a constant value of one, reorganizing the data using p^* and t^* does collapse all the data into a single curve. The deviation of this curve from a straight line is similar to that seen in the dimensional plots and is due to multidimensional effects.

SUMMARY AND CONCLUDING REMARKS

The proposal to use slush hydrogen as the propellant storage medium for the NASP presents a formidable challenge to the design and efficient operation of the propellant management system. Previous studies of propellant tank pressurization prior to main engine ignition have primarily involved experimental measurements in model tanks^{1,2} or analytical and computational models based on lumped or one-dimensional

models⁴. The present study was initiated: to develop a capability for multidimensional modeling of the propellant tank pressurization process prior to main engine ignition; to evaluate the performance of, and identify limitations in, the model and; to begin evaluation of the parametric dependence of the pressurization process on the system initial conditions and boundary conditions.

After a review of available computational tools, the FLOW-3D code was selected as the most promising candidate for modeling pressurization and expulsion of slush hydrogen from storage tanks. Code performance was evaluated by comparing computational predictions to measurements obtained during the pressurization of an experimental simulation of a NASP propellant tank¹. The analyses demonstrated that, despite significant uncertainties in problem definition due to incomplete specification of the experiment conditions, a pie-sector (axisymmetric) computational model was able to replicate the tank pressure history and to predict the total pressurant mass required for the pressurization to within 15% of the measured value. Based on this evaluation, it was concluded that FLOW-3D is a suitable tool from multidimensional modeling of the pressurization process.

Typical of many efforts to verify computational tools by comparison to experiment data not specifically obtained for this purpose, the performance evaluation was complicated by the absence from the experiment report of key parameters required to define the model. To help eliminate uncertainties in model definition, future experiments should include measurement of: the history of pressurant inlet pressure, temperature, and mass flow rate; the initial temperature distribution within the ullage; the history of heat loss to the tank wall and to the slush/vapor interface and; the rate of evaporation or condensation at the free surface. Measurements necessary to evaluate code performance should include the pressure history in the tank and the transient velocity and temperature fields in the ullage during pressurization. Although it is recognized that the distinction between model definition and performance evaluation

measurements is tenuous, and that some of the requested measurements are difficult to obtain, the lists have been assembled as a starting point for consideration by future efforts.

The dependence of the pressurization process on initial ullage temperature distribution was examined by comparing predictions for a 60-40 °R distribution, representing a well mixed initial condition, to those for a 250-40 °R distribution, representing a thermally stratified initial condition. For the pressurant mass flow rates considered and the heat flux rate specified at the ullage boundary, the global performance as measured by elapsed time required for the pressurization and the total pressurant mass added appears to be nearly independent of the initial ullage temperature distribution. Review of the predicted velocity and temperature fields near the free surface at the end of pressurization indicates that the assumption of no mass transfer at this interface merits future scrutiny. Further, the specification of a single heat flux rate at the tank wall for all cases is also suspect and should be replaced by a more accurate model when possible.

A study of the effect of pressurant mass flow rate on the pressurization process revealed an interesting trend as well as potentially significant differences between pressurization of liquid hydrogen and pressurization of slush hydrogen. For both liquid and slush cases, the pressurant mass required to reach the desired pressure level decreases with increasing pressurant mass flow rate. This is in accord with experiment data¹ and is discussed in detail in the preceding section. Review of the temperature and velocity fields predicted for the slush and liquid cases during this study revealed interesting differences between the cases. At comparable pressurant mass flow rates, the inlet jet fully penetrates the ullage of the slush cases whereas it does not for the liquid cases. This difference leads to significantly different flow and temperature fields in the ullage. The temperature field predicted for the liquid cases has little radial dependence and the one-dimensional model provided by the SLURP code⁴ is probably reasonable. In

contrast, the temperature fields predicted for pressurization of slush have a very significant radial dependency and will not be well represented by a one-dimensional model. Further, at the higher mass flow rates, the temperatures and velocities near the free surface of the slush are significantly higher for the slush cases than for the liquid cases. The low values predicted for the liquid cases suggest that the assumption of no mass transfer at the free surface may be reasonable whereas the high values for the slush case cast serious doubt on the validity of such an assumption.

A simplified model of the pressurization process was developed in search of a nondimensional characterization of the process. Based on this model, a dimensionless time was defined as elapsed time from pressurization initiation normalized by the time required to complete pressurization. A dimensionless pressure was defined by the increase in pressure from initial pressure divided by the total pressure rise to be accomplished. Using these dimensionless parameters, it was demonstrated that the tank pressure history for all of the cases in this study collapse into a single curve. Although the relationship revealed by this study lacks predictive capability since the dimensionless parameters contain variables which are not known a priori, it is valuable for unifying the presentation of data from experimental and computational studies of the pressurization process.

ACKNOWLEDGMENTS

This research was made possible by the support of the NASA Lewis Research Center provided through NASA Grant NAG3-1156.

REFERENCES

¹ Stochl, R.J., "Gaseous Hydrogen Requirements for the Discharge of Liquid Hydrogen from a 1.52 m (5ft) Diameter Spherical Tank", NASA TND-5336, August 1969.

² Stochl, R.J., "Gaseous Helium Requirements for the Discharge of Liquid Hydrogen from a 1.52 m (5ft) Diameter Spherical Tank", NASA TND-5621, January 1970.

³ Aydelott, J.C., Carney, M.J., and Hochstein, J.I., "NASA Lewis Research Center Low-Gravity Fluid Management Technology Program," NASA TM-87145, November 1985.

⁴ Hardy, T.L. and Thomsik, T.M., "SLURP: A Computer Code for Pressurization of a Slush Hydrogen Tank Using Gaseous Hydrogen or Helium," NASP TM-1088, January 1990.

⁵ Hardy, T.L. and Tomsik, T.M., "Prediction of Ullage Gas Thermal Stratification in a NASP Vehicle Propellant Tank Experimental Simulation Using FLOW-3D," NASA TM-103217, July 1990.

⁶ FLOW3D: Computational Modeling Power for Scientists and Engineers," Flow Science Inc, Los Alamos, New Mexico, 1988.

⁷ Navikas, J., Cady, E.C., Flaska, T.L., "Modeling of Solid-Liquid Circulation in National Aerospace Plane's Slush Hydrogen Tanks", 24th Joint Propulsion Conference, Boston, Massachusetts, 11-14 July 1988.

⁸ Hochstein, J.I., "Computational Prediction of Propellant Motion During Separation of a Centaur G-Prime Vehicle From the Shuttle", Report No. WU/CFDL-85/1, Washington University, St. Louis, December 1985.

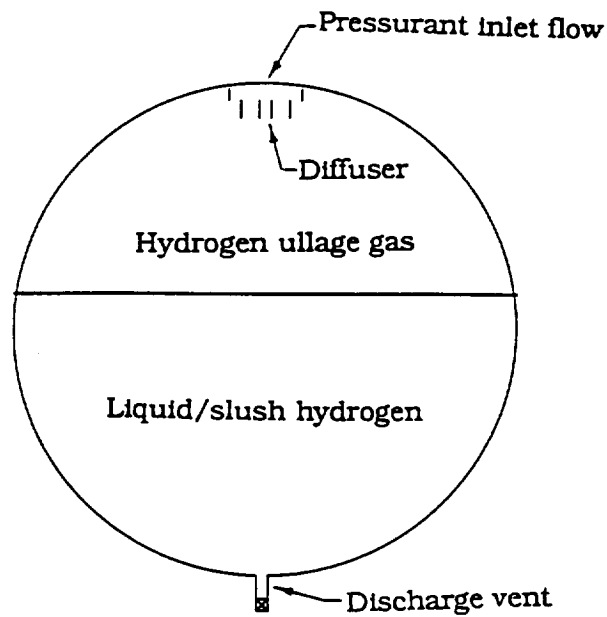


Figure 1 Schematic of experiment tank

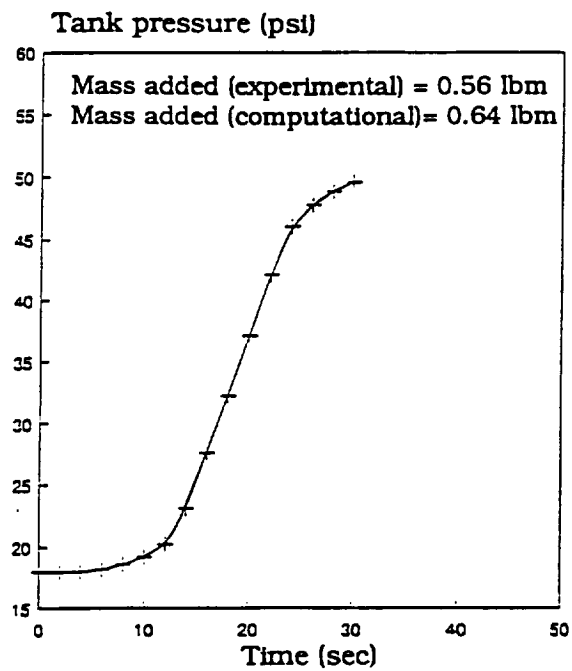
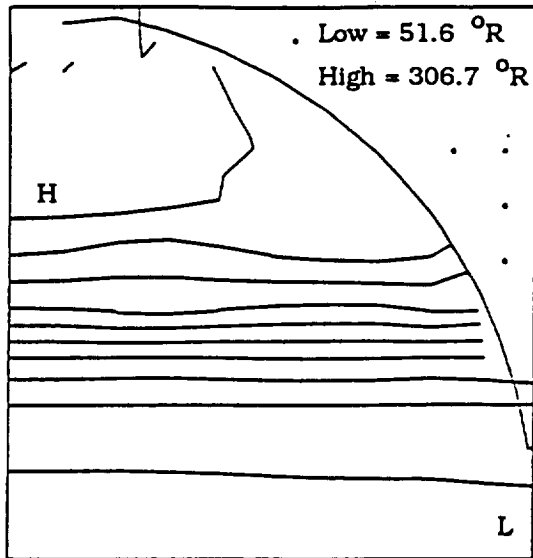
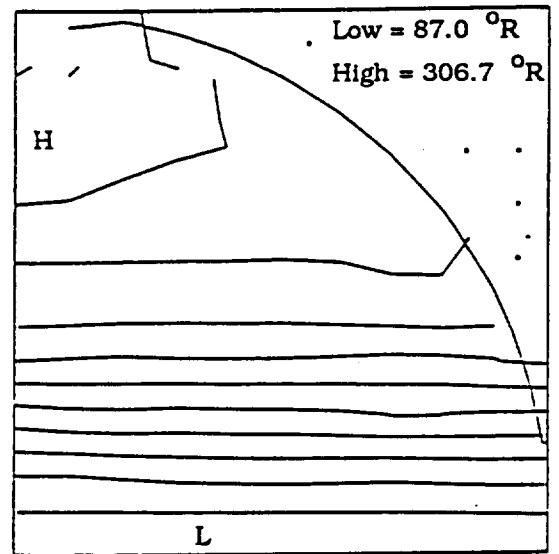


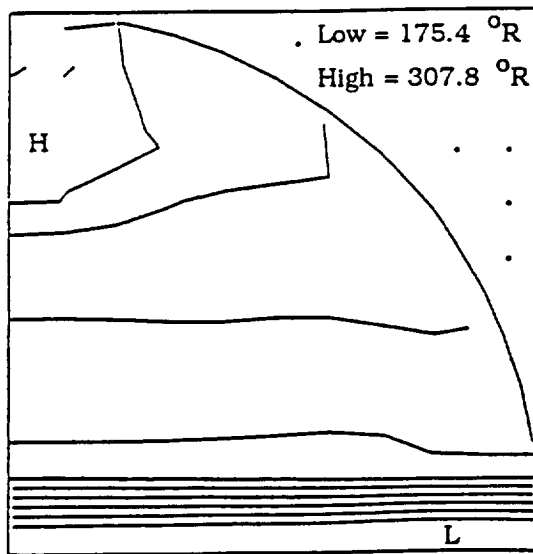
Figure 2 Pressurization of tank containing liquid hydrogen (55.6 % ullage)



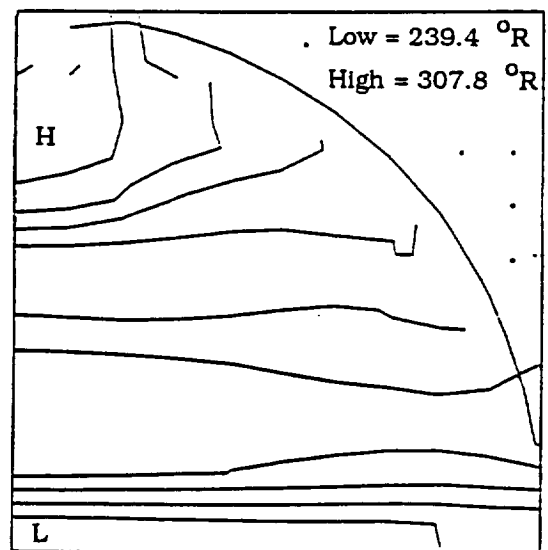
(a) Case # 4



(b) Case # 3



(c) Case # 5



(d) Case # 6

Figure 3 Temperature distribution at the end of pressurization ($\dot{m} = 0.277$ lbm/s)

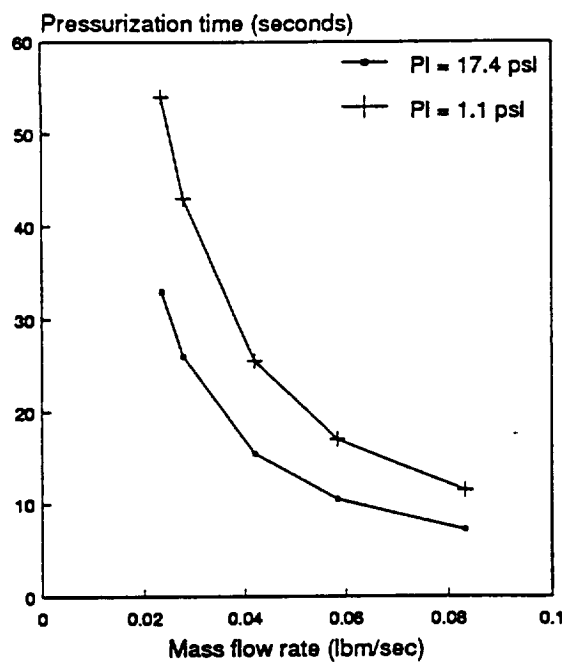


Figure 4 Pressurization time .vs. Mass flow rate

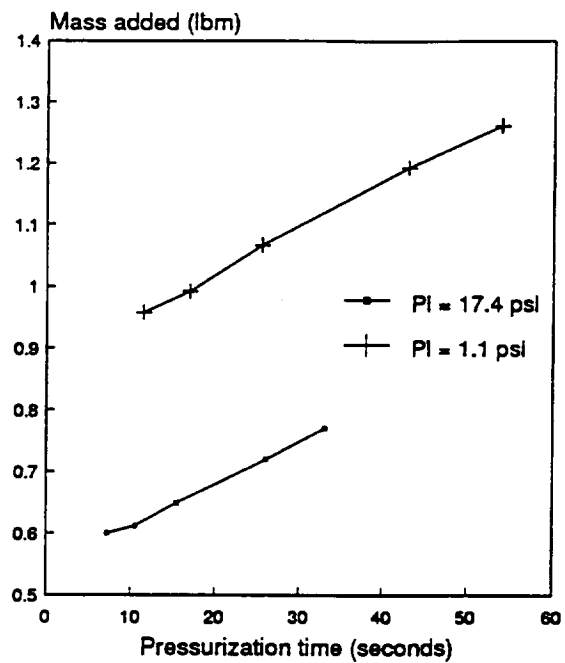


Figure 5 Mass added .vs. Pressurization time

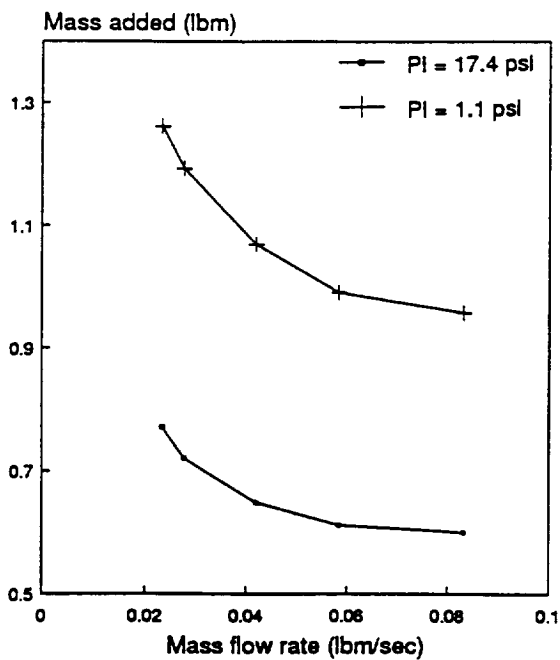
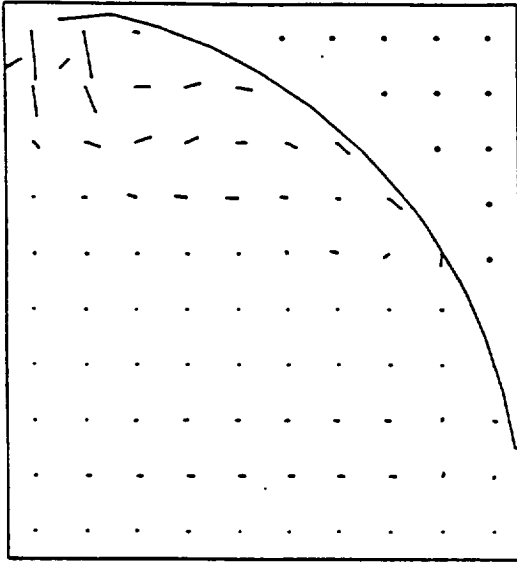
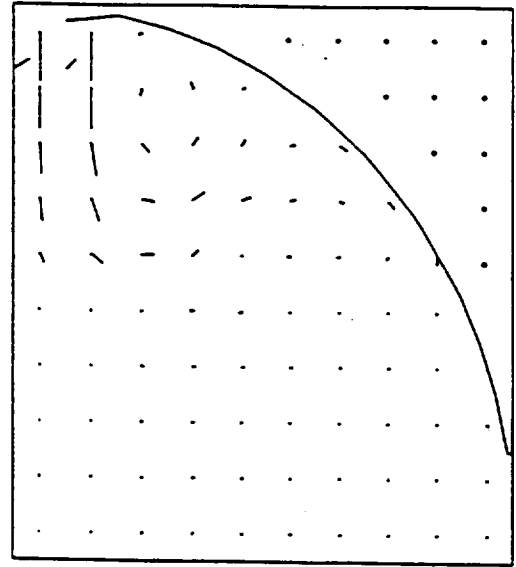


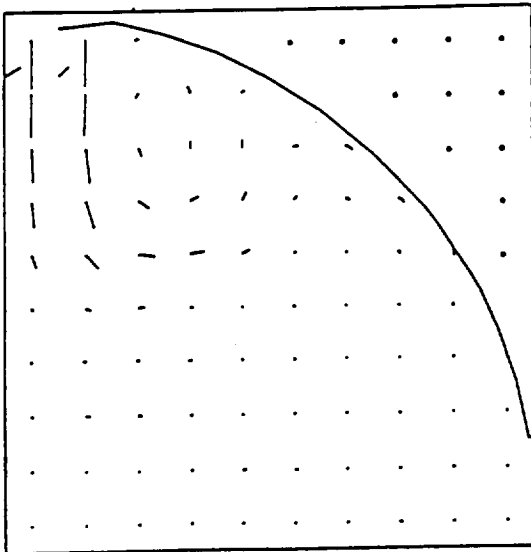
Figure 6 Mass added .vs. Mass flow rate



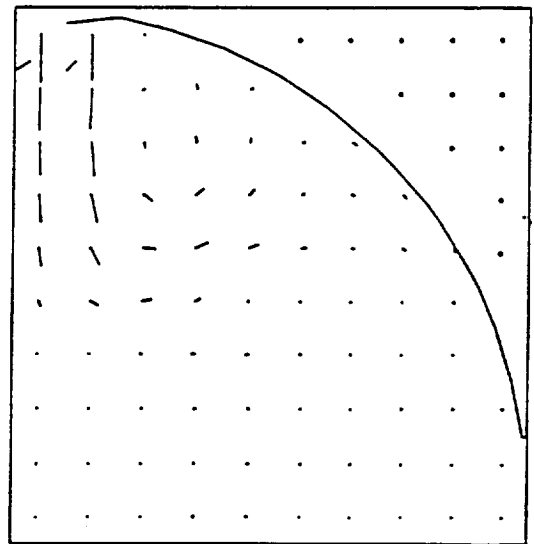
(a) Case # 1



(b) Case # 7

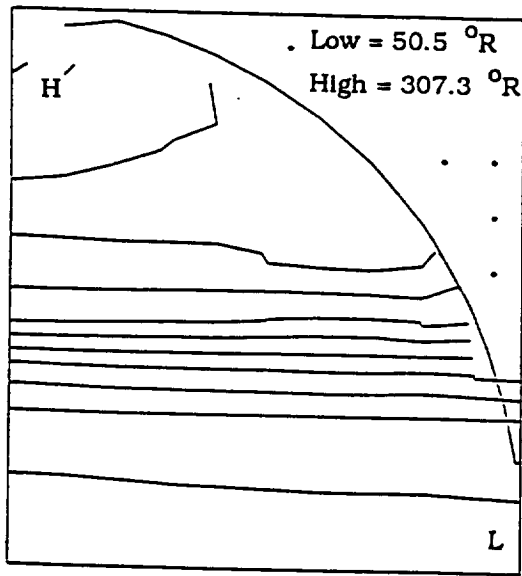


(c) Case # 9

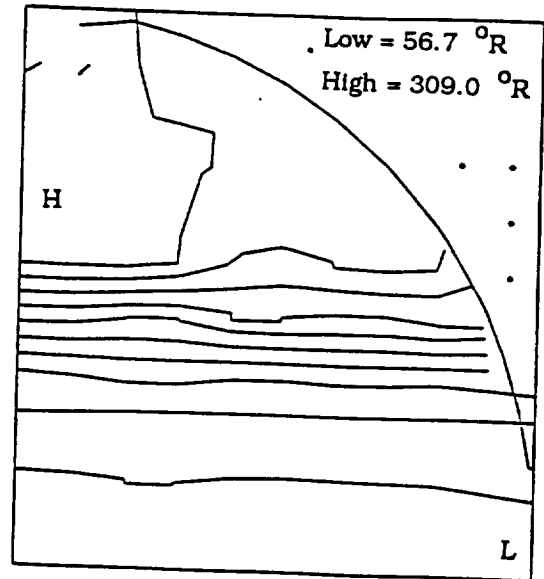


(d) Case # 11

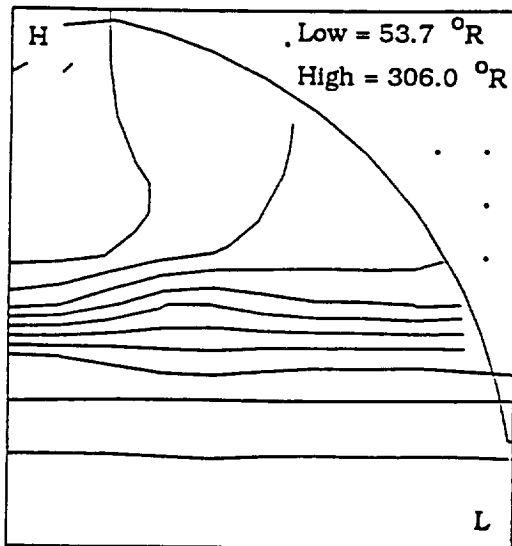
Figure 7 Velocity fields for pressurizing liquid hydrogen



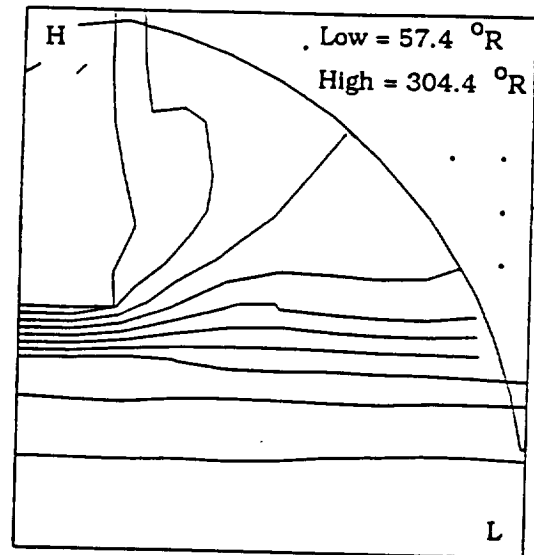
(a) Case # 1



(b) Case # 7

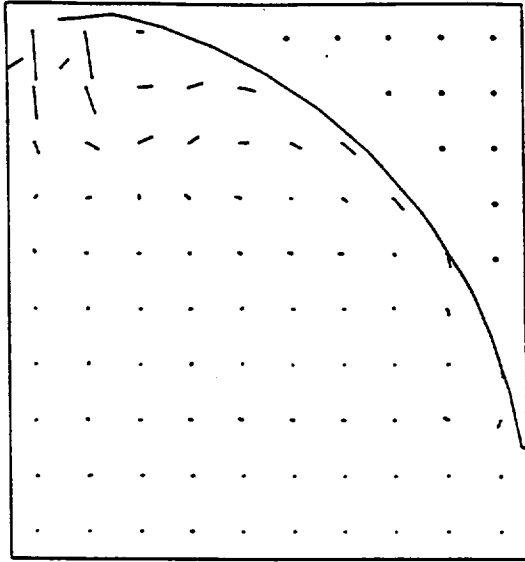


(c) Case # 9

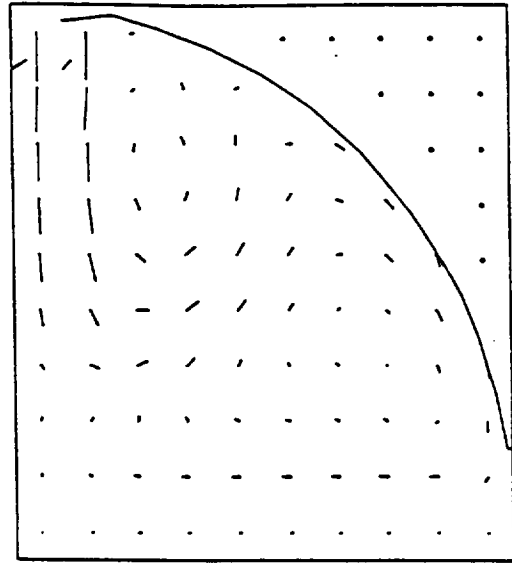


(d) Case # 11

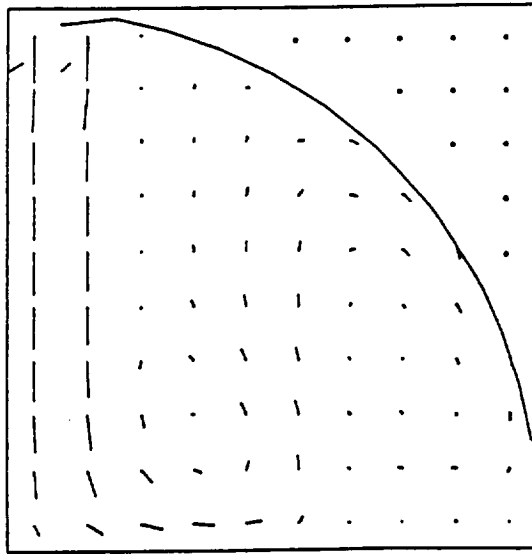
Figure 8 Temperature fields for pressurizing liquid hydrogen



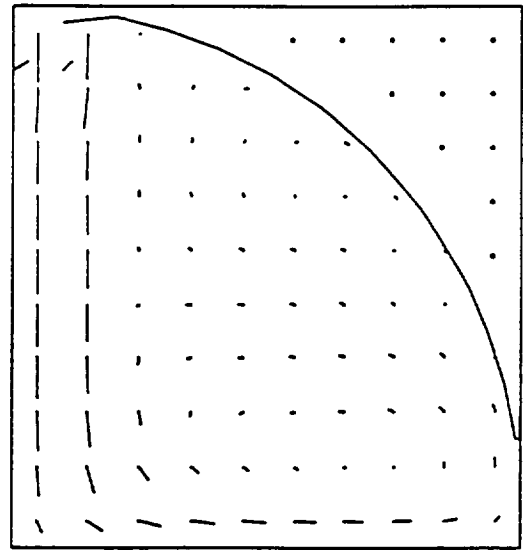
(a) Case # 2



(b) Case # 8

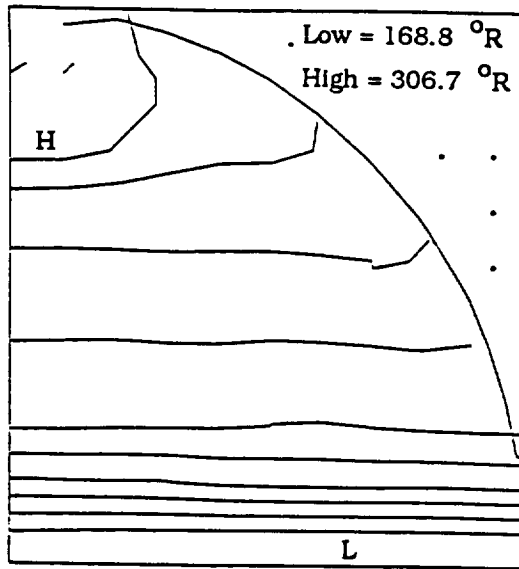


(c) Case # 10

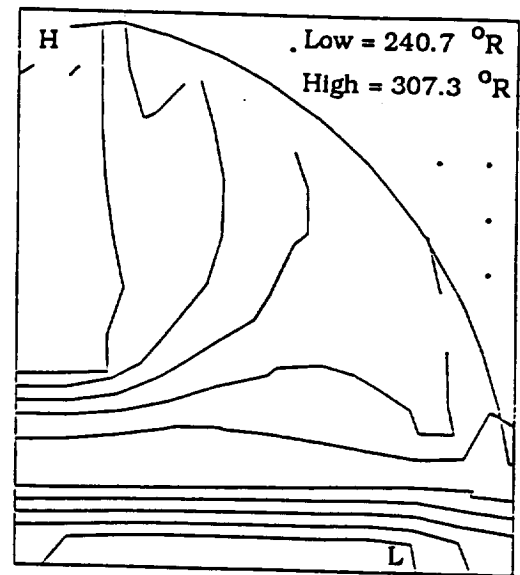


(d) Case # 12

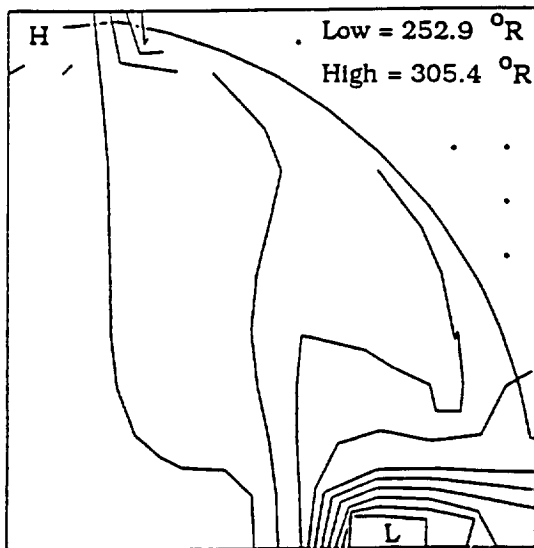
Figure 9 Velocity fields for pressurizing slush hydrogen



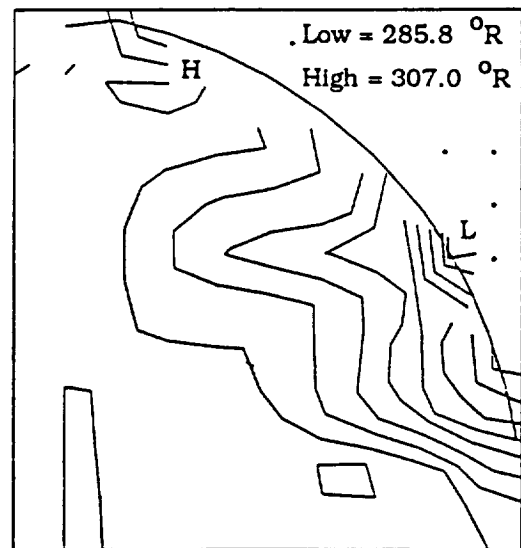
(a) Case # 2



(b) Case # 8



(c) Case # 10



(d) Case # 12

Figure 10 Temperature fields for pressurizing liquid hydrogen

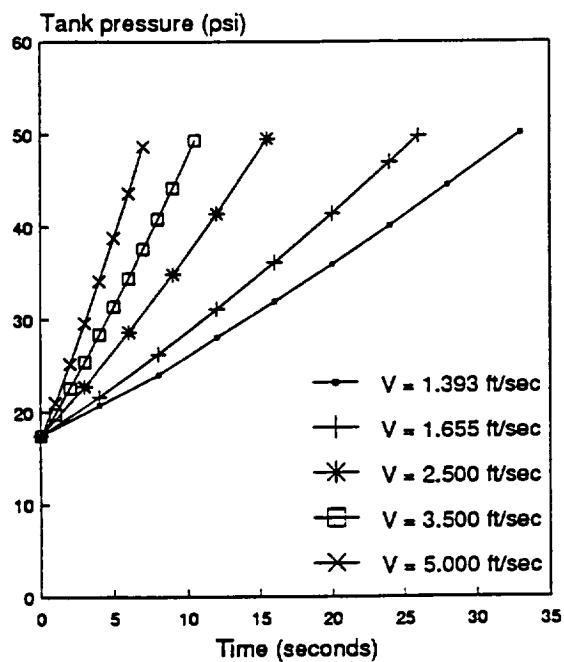


Figure 11 Tank pressure history
(liquid hydrogen)

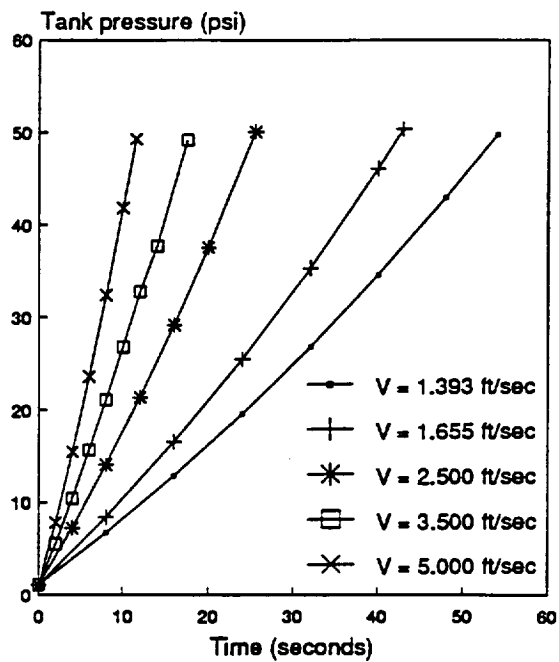


Figure 12 Tank pressure history
(slush hydrogen)

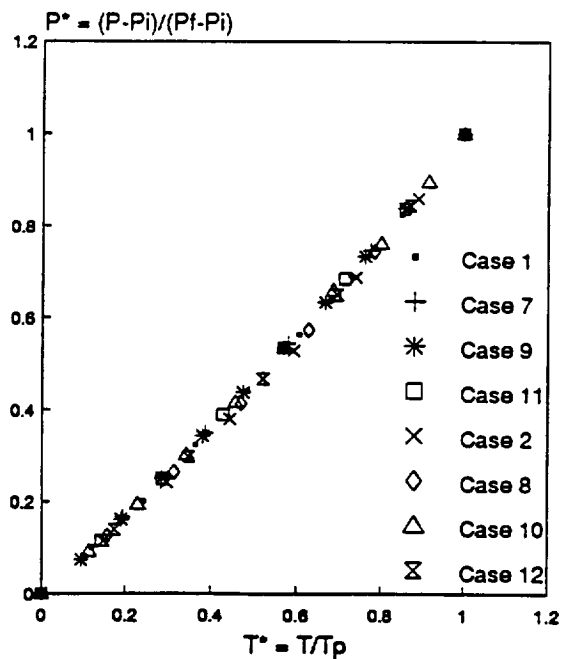


Figure 13 Dimensionless pressure .vs.
normalized time

1. **Introduction**
 2. **Background**
 3. **Methodology**
 4. **Results**
 5. **Discussion**
 6. **Conclusion**
 7. **References**
 8. **Appendix**
 9. **Figure 1**
 10. **Figure 2**
 11. **Figure 3**
 12. **Figure 4**
 13. **Figure 5**
 14. **Figure 6**
 15. **Figure 7**
 16. **Figure 8**
 17. **Figure 9**
 18. **Figure 10**
 19. **Figure 11**
 20. **Figure 12**
 21. **Figure 13**
 22. **Figure 14**
 23. **Figure 15**
 24. **Figure 16**
 25. **Figure 17**
 26. **Figure 18**
 27. **Figure 19**
 28. **Figure 20**
 29. **Figure 21**
 30. **Figure 22**
 31. **Figure 23**
 32. **Figure 24**
 33. **Figure 25**
 34. **Figure 26**
 35. **Figure 27**
 36. **Figure 28**
 37. **Figure 29**
 38. **Figure 30**
 39. **Figure 31**
 40. **Figure 32**
 41. **Figure 33**
 42. **Figure 34**
 43. **Figure 35**
 44. **Figure 36**
 45. **Figure 37**
 46. **Figure 38**
 47. **Figure 39**
 48. **Figure 40**
 49. **Figure 41**
 50. **Figure 42**
 51. **Figure 43**
 52. **Figure 44**
 53. **Figure 45**
 54. **Figure 46**
 55. **Figure 47**
 56. **Figure 48**
 57. **Figure 49**
 58. **Figure 50**
 59. **Figure 51**
 60. **Figure 52**
 61. **Figure 53**
 62. **Figure 54**
 63. **Figure 55**
 64. **Figure 56**
 65. **Figure 57**
 66. **Figure 58**
 67. **Figure 59**
 68. **Figure 60**
 69. **Figure 61**
 70. **Figure 62**
 71. **Figure 63**
 72. **Figure 64**
 73. **Figure 65**
 74. **Figure 66**
 75. **Figure 67**
 76. **Figure 68**
 77. **Figure 69**
 78. **Figure 70**
 79. **Figure 71**
 80. **Figure 72**
 81. **Figure 73**
 82. **Figure 74**
 83. **Figure 75**
 84. **Figure 76**
 85. **Figure 77**
 86. **Figure 78**
 87. **Figure 79**
 88. **Figure 80**
 89. **Figure 81**
 90. **Figure 82**
 91. **Figure 83**
 92. **Figure 84**
 93. **Figure 85**
 94. **Figure 86**
 95. **Figure 87**
 96. **Figure 88**
 97. **Figure 89**
 98. **Figure 90**
 99. **Figure 91**
 100. **Figure 92**
 101. **Figure 93**
 102. **Figure 94**
 103. **Figure 95**
 104. **Figure 96**
 105. **Figure 97**
 106. **Figure 98**
 107. **Figure 99**
 108. **Figure 100**
 109. **Figure 101**
 110. **Figure 102**
 111. **Figure 103**
 112. **Figure 104**
 113. **Figure 105**
 114. **Figure 106**
 115. **Figure 107**
 116. **Figure 108**
 117. **Figure 109**
 118. **Figure 110**
 119. **Figure 111**
 120. **Figure 112**
 121. **Figure 113**
 122. **Figure 114**
 123. **Figure 115**
 124. **Figure 116**
 125. **Figure 117**
 126. **Figure 118**
 127. **Figure 119**
 128. **Figure 120**
 129. **Figure 121**
 130. **Figure 122**
 131. **Figure 123**
 132. **Figure 124**
 133. **Figure 125**
 134. **Figure 126**
 135. **Figure 127**
 136. **Figure 128**
 137. **Figure 129**
 138. **Figure 130**
 139. **Figure 131**
 140. **Figure 132**
 141. **Figure 133**
 142. **Figure 134**
 143. **Figure 135**
 144. **Figure 136**
 145. **Figure 137**
 146. **Figure 138**
 147. **Figure 139**
 148. **Figure 140**
 149. **Figure 141**
 150. **Figure 142**
 151. **Figure 143**
 152. **Figure 144**
 153. **Figure 145**
 154. **Figure 146**
 155. **Figure 147**
 156. **Figure 148**
 157. **Figure 149**
 158. **Figure 150**
 159. **Figure 151**
 160. **Figure 152**
 161. **Figure 153**
 162. **Figure 154**
 163. **Figure 155**
 164. **Figure 156**
 165. **Figure 157**
 166. **Figure 158**
 167. **Figure 159**
 168. **Figure 160**
 169. **Figure 161**
 170. **Figure 162**
 171. **Figure 163**
 172. **Figure 164**
 173. **Figure 165**
 174. **Figure 166**
 175. **Figure 167**
 176. **Figure 168**
 177. **Figure 169**
 178. **Figure 170**
 179. **Figure 171**
 180. **Figure 172**
 181. **Figure 173**
 182. **Figure 174**
 183. **Figure 175**
 184. **Figure 176**
 185. **Figure 177**
 186. **Figure 178**
 187. **Figure 179**
 188. **Figure 180**
 189. **Figure 181**
 190. **Figure 182**
 191. **Figure 183**
 192. **Figure 184**
 193. **Figure 185**
 194. **Figure 186**
 195. **Figure 187**
 196. **Figure 188**
 197. **Figure 189**
 198. **Figure 190**
 199. **Figure 191**
 200. **Figure 192**
 201. **Figure 193**
 202. **Figure 194**
 203. **Figure 195**
 204. **Figure 196**
 205. **Figure 197**
 206. **Figure 198**
 207. **Figure 199**
 208. **Figure 200**
 209. **Figure 201**
 210. **Figure 202**
 211. **Figure 203**
 212. **Figure 204**
 213. **Figure 205**
 214. **Figure 206**
 215. **Figure 207**
 216. **Figure 208**
 217. **Figure 209**



100
A 22681

AIAA 93-0278

Influence of Heat Transfer Rates on Pressurization of Liquid/Slush Hydrogen Propellant Tanks

G. P. Sasmal, J. I. Hochstein
Memphis State University
Memphis, Tennessee

and

T. L. Hardy
NASA Lewis Research Center
Cleveland, Ohio

**31st Aerospace Sciences
Meeting & Exhibit**
January 11-14, 1993 / Reno, NV

INFLUENCE OF HEAT TRANSFER RATES ON PRESSURIZATION OF LIQUID/SLUSH HYDROGEN PROPELLANT TANKS

G. P. Sasmal*, J. I. Hochstein**

Memphis State University, Memphis, Tennessee 38152

T. L. Hardy***

NASA Lewis Research Center, Cleveland, Ohio 44135

ABSTRACT

A multi-dimensional computational model of the pressurization process in liquid/slush hydrogen tank is developed and used to study the influence of heat flux rates at the ullage boundaries on the process. The new model computes these rates and performs an energy balance for the tank wall whereas previous multi-dimensional models required a priori specification of the boundary heat flux rates. Analyses of both liquid hydrogen and slush hydrogen pressurization were performed to expose differences between the two processes. Graphical displays are presented to establish the dependence of pressurization time, pressurant mass required, and other parameters of interest on ullage boundary heat flux rates and pressurant mass flow rate. Detailed velocity fields and temperature distributions are presented for selected cases to further illuminate the details of the pressurization process. It is demonstrated that ullage boundary heat flux rates do significantly effect the pressurization process and that minimizing heat loss from the ullage and maximizing pressurant flow rate minimizes the mass of pressurant gas required to pressurize the tank. It is further demonstrated that proper dimensionless scaling of pressure and time permit all the pressure histories examined during this study to be displayed as a single curve.

NOMENCLATURE

A	area
h	heat transfer coefficient
MC	mass-specific heat product
p	pressure
p_i	initial pressure
p_f	final pressure
P^*	dimensionless pressure
t	time
t_f	pressurization time
t^*	dimensionless time
T	temperature
T_w	tank wall temperature
Q_w	rate of heat transfer from ullage to tank wall
Q_l	rate of heat transfer from ullage to liquid/slush

INTRODUCTION

For the past several years, the pressurization process in cryogenic propellant tanks has been the focus of several analytical^{1,2}, experimental^{2,3}, and numerical studies⁴. Design and efficient operation of liquid/slush hydrogen propellant tanks (such as proposed for the National Aerospace Plane), requires the ability to accurately model this process. The use of slush hydrogen propellant makes this a particularly challenging task because it requires the modeling of transient fluid mechanic and thermodynamic processes in the presence of all three phases of matter. The flow field and the temperature field in a tank during pressurization are multi-dimensional and it is likely that the tank will be subject to multi-dimensional environmental influences. Existing models are fundamentally one dimensional and based on simplifying assumptions and experimentally derived correlations. Although one-dimensional models may be satisfactory for preliminary design studies, it is not clear that they are adequate as design tools for future vehicle development. Sasmal, Hochstein, and Wendl⁴ reported a multi-dimensional model for such a process using the FLOW-3D code⁵ and demonstrated its accuracy by comparing computational predictions to experimentally obtained data. They simplified the heat transfer models at the ullage boundaries by specifying constant heat flux rates predicted by a one-dimensional model, (the SLURP code)¹, to study the parametric dependencies of the pressurization process. Although a reasonable first approximation, this assumption is suspect because the process itself is transient and is influenced by several parameters which have values that change during the pressurization process.

The present study was undertaken to more accurately model the heat transfer at the ullage boundaries and to investigate its effect on the pressurization process. Although the predictions of the present model are in qualitative agreement with previously published data⁴, the quantitative differences produced by the improved transient heat flux rates at the ullage boundaries clearly indicate the strong dependency of the pressurization process in liquid and slush propellant tanks on these quantities.

* Research Associate, Mechanical Engr., Member AIAA

** Associate Professor, Mechanical Engr., Assoc. Fellow AIAA

*** Aerospace Engineer, Member AIAA.

PROPELLANT TANK CONFIGURATION

The geometric configuration used in the present study is a partially filled 5 ft diameter spherical aluminum tank with a wall thickness of 0.3 inch. A schematic of this configuration is presented in Fig. 1.

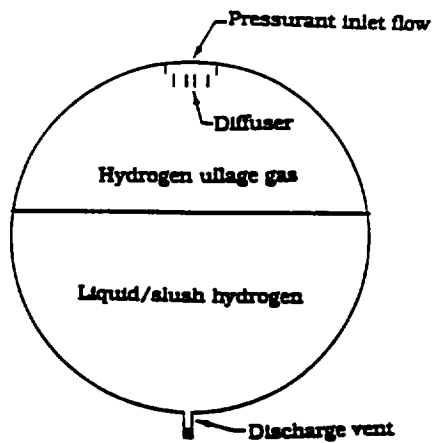


Figure 1 Schematic of experiment tank

The tank is pressurized by injecting gaseous hydrogen through a 1 ft diameter diffuser located at the top of the tank until the tank pressure reaches 50 psi. The initial vapor pressure is 17.4 psi when pressurizing liquid hydrogen and 1.1 psi when pressurizing slush hydrogen. These specifications were adopted from an experimental study⁶ so that computational predictions could be compared to experimentally obtained data for the pressurization process.

COMPUTATIONAL MODEL

The FLOW-3D code⁵ was selected as the computational tool to provide multi-dimensional modeling of the pressurization process. Since the configuration of interest is an axisymmetric geometry, and the present study is focused on axisymmetric boundary conditions, a pie sector model (10x1x10 mesh) was selected to reduce the computational demands for completing the study. Pie-sector model performance, computational grid convergence, and the suitability of FLOW-3D for modeling the pressurization process in liquid/slush hydrogen propellant tanks has already been documented⁴. A previous pressurization study⁴ enforced constant heat flux rates at the ullage boundaries that were obtained from a one-dimensional model¹. More accurate modeling of these boundary conditions was achieved in the present study by dividing the tank wall into azimuthal strips and identifying each as a separate obstacle. The code provides an option to model each obstacle as a thermal lump and can compute the temperature of each obstacle using the expression:

$$MC \frac{dT_w}{dt} = hA(T - T_w) \quad (1)$$

where MC is the mass-specific heat product, A is the obstacle surface area, h is the heat transfer coefficient, T_w is the obstacle temperature, and T is the fluid temperature in the adjacent cell. The code computes values for h based on correlations⁵ for natural convection, forced convection, and conduction within the fluid and then uses the largest value when computing the wall temperature.

ANALYSES, RESULTS, AND DISCUSSION

The primary goal of the present study is to examine the dependence of the pressurization process on the heat transfer rates from the ullage to the tank wall and to the liquid/slush pool. The traditional approach to multivariable problems, (varying one parameter at a time), was used to study the sensitivity of the pressurization process to "assumptions" as well as traditional "control" variables. Where available, the initial and boundary conditions specified for the analyses were those measured during the corresponding experimental study⁶. Although a detailed axial temperature distribution was not measured during the experimental study, the initial temperature in the ullage is approximated by a linear variation from 250° R at the inlet diffuser to 40° R at the phase interface. The initial tank wall temperature was therefore specified to vary linearly from 220° R at the diffuser to 40° R at the interface. The inlet gas temperature was a constant 307° R and the inlet pressure was maintained at 50 psi. A constant rate of heat flux per unit area from the environment to the tank (0.00884 Btu/sec-ft²) was specified. To simplify the present study, no evaporation/condensation at the liquid/slush-vapor interface was assumed. All analyses were performed for an ullage volume fraction of 0.556. Using this model, analyses were performed for pressurization of a liquid and a slush propellant tank to reveal differences in their response to similar boundary conditions.

To expose the sensitivity of the pressurization process to the heat transfer rate from the ullage to the tank wall and to the liquid/slush-vapor interface, a sequence of analyses were performed. The first analysis used the same heat transfer rates computed by a one-dimensional SLURP model¹ that were used in the previous study⁴. The second analysis retained the same liquid/slush-vapor interface heat transfer rate, but enforced an adiabatic boundary at the tank wall. Although this is not an improvement in the fidelity of the model, it is useful as an extreme condition for examining the sensitivity of the pressurization process to this parameter. The third analysis used the obstacle heat storage model for the tank wall and a specified temperature boundary condition to model the liquid/slush-vapor interface. The linear temperature variation discussed above was used to initialize the tank wall obstacles and the liquid/slush-vapor interface was specified to be a constant 40° R. Figure 2 displays the relationship between required pressurant mass and pressurant mass flow rate for

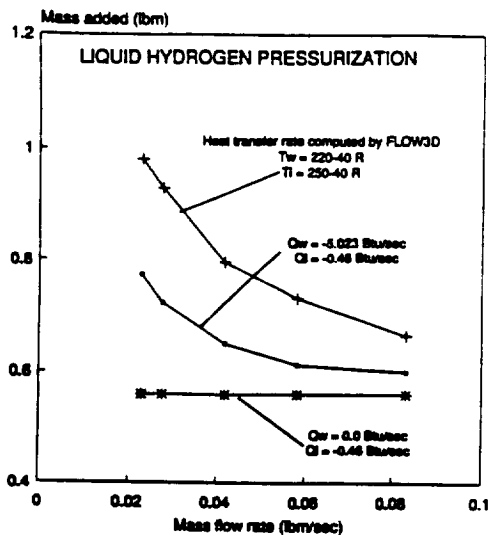


Figure 2 Mass added vs. Mass flow rate (liquid)

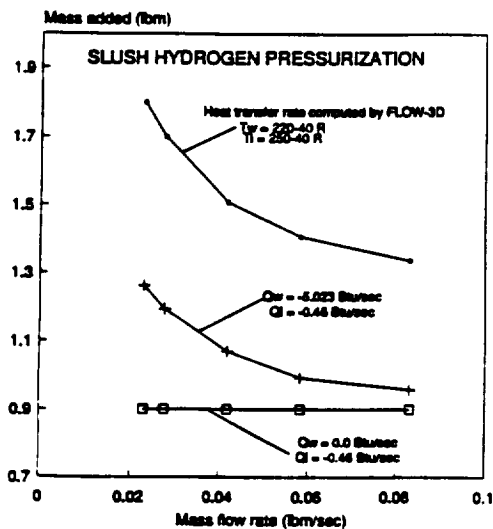


Figure 3 Mass added vs. Mass flow rate (slush)

pressurization of a liquid propellant tank using the three different heat transfer boundary conditions. Figure 3 displays the corresponding information for pressurization of a slush propellant tank. The cases with heat transfer rate computed by FLOW-3D have higher heat losses than the other cases and reveal a decrease in required pressurant mass with decrease in the rate of heat loss from the ullage. With no heat loss to the tank wall, and 0.46 Btu/sec heat loss rate to the liquid/slush hydrogen, pressurant mass required was nearly constant for all mass flow rates. Results from analyses with heat transfer to the tank wall show a decreased pressurant mass requirement with increasing mass flow rate. Comparing cases with similar boundary models, the slush hydrogen consistently requires more pressurant mass than the liquid to reach 50 psi. Review of the results from these analyses leads to the conclusion that the more detailed model consistently

predicts a larger required pressurant mass and is therefore conservative for design purposes.

The tank wall temperature distribution predicted at the end of pressurization for different inlet mass flow rates, using the obstacle heat storage model, are presented in Figs. 4 and 5 for liquid and slush hydrogen respectively.

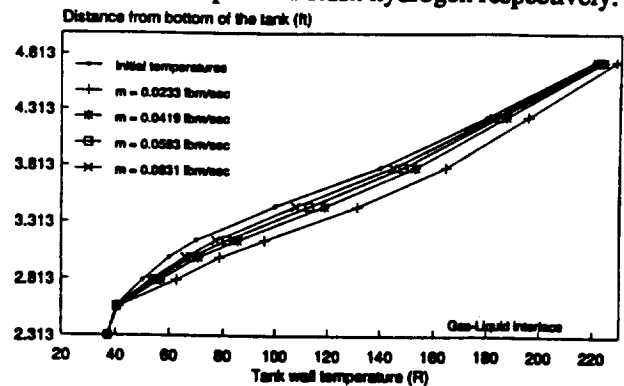


Figure 4 Wall temperature distribution (liquid)

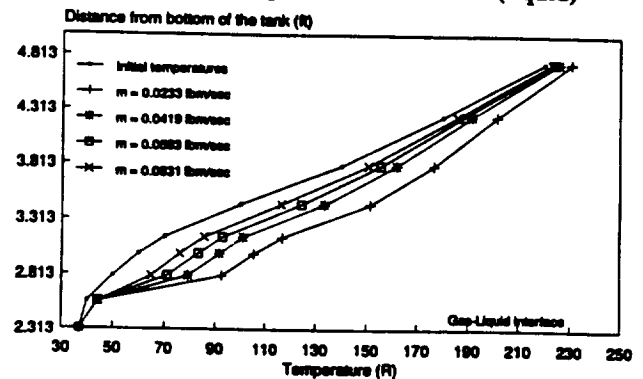


Figure 5 Wall temperature distribution (slush)

The final tank wall temperature distributions show that higher temperatures are predicted for the slush case than for the liquid case. This difference is believed to be due to the longer pressurization time required for the slush case and a significantly different flow pattern in the ullage for the two cases. Figures 6 and 7 display the predicted temperature distributions along the tank centerline at the end of the pressurization period for liquid and for slush hydrogen respectively. These figures clearly display the extent of penetration of the hot gas into the cold ullage and reveal significantly greater penetration for the slush case than for the liquid case. This interpretation is further substantiated by detailed velocity and temperature fields discussed later.

The influence of pressurant mass flow rate on the rate of heat loss from the ullage to the tank wall is displayed in Fig. 8 for pressurization of liquid hydrogen and Fig. 9 for pressurization of slush hydrogen. These profiles were predicted using the obstacle heat storage model. For both cases, the rate of heat loss increases with increasing time and increases more rapidly at higher inflow rates. This is reasonable, since higher mass flow rates should result in a higher heat transfer coefficient at the wall.

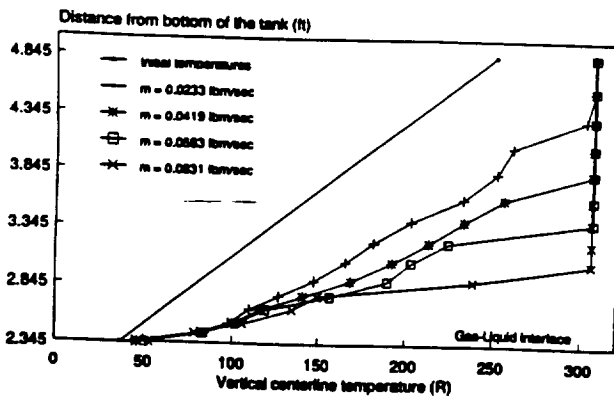


Figure 6 Ullage temperature distribution (liquid)

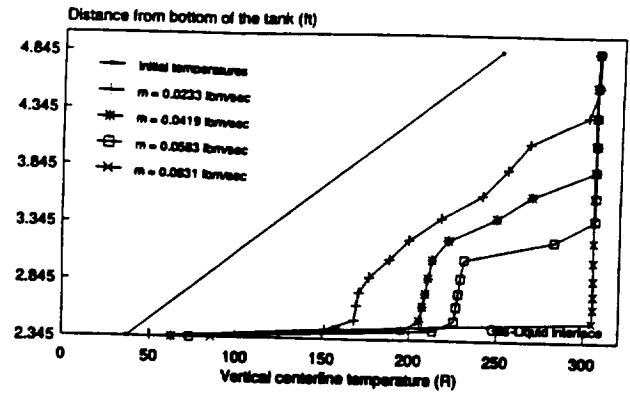


Figure 7 Ullage temperature distribution (slush)

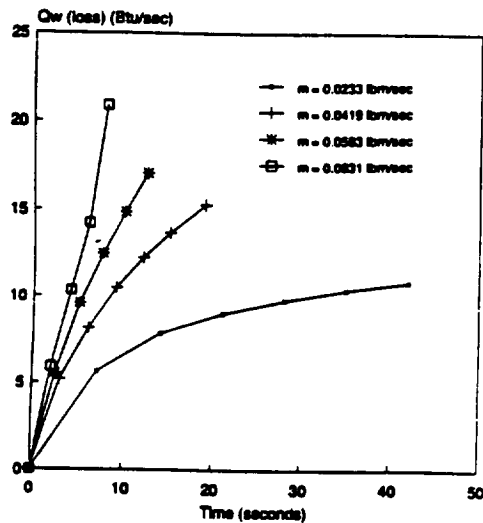


Figure 8 Heat transfer rate from ullage to tank wall (liquid)

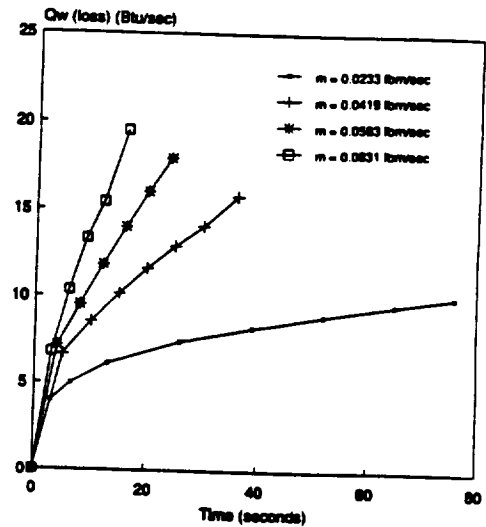


Figure 9 Heat transfer rate from ullage to tank wall (slush)

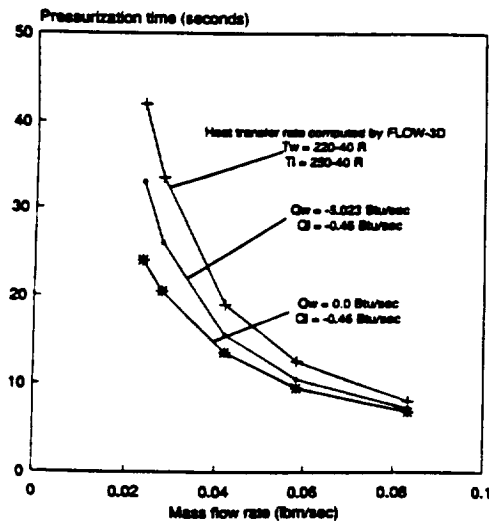


Figure 10 Pressurization time (liquid)

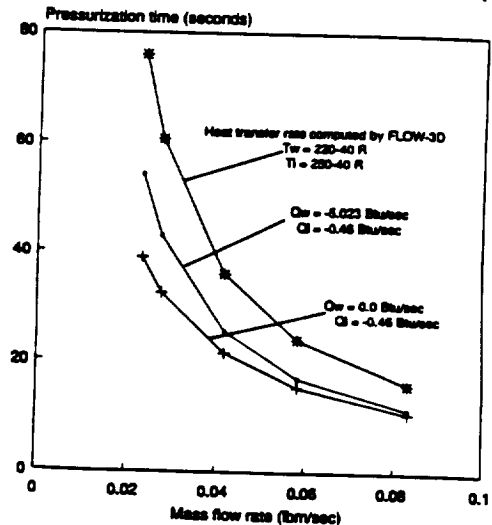


Figure 11 Pressurization time (slush)

Figures 10 and 11 (liquid and slush) display a decrease in pressurization time with increase in mass flow rate as one would expect from a cursory analysis. The increased heat loss rates computed using the obstacle heat storage model as compared to the other models result in increased pressurization times.

Velocity and temperature fields predicted for slush and for liquid hydrogen pressurization using the obstacle heat storage model are depicted in Figs. 12-15. These fields are different from each other and from those predicted using SLURP-based constant boundary heat flux rates⁴. Comparing the predicted fields reveals significant

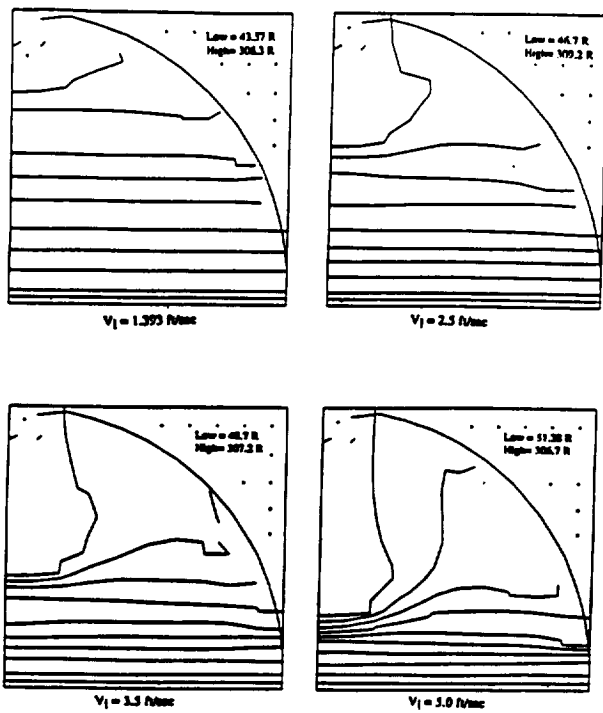


Figure 12 End of pressurization temperature fields (liquid)

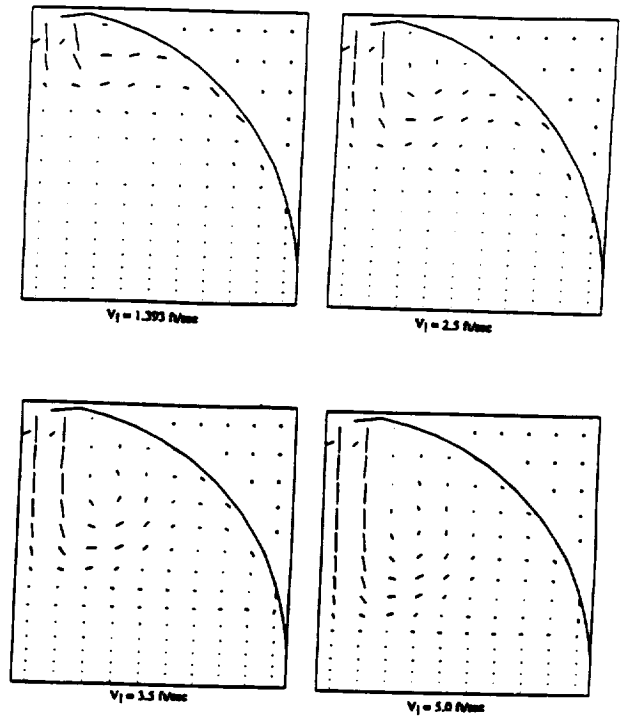


Figure 13 End of pressurization velocity fields (liquid)

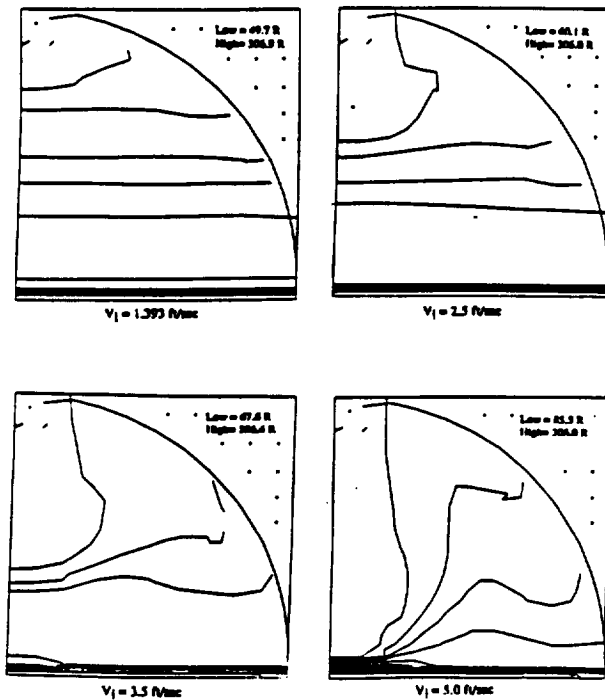


Figure 14 End of pressurization temperature fields (slush)

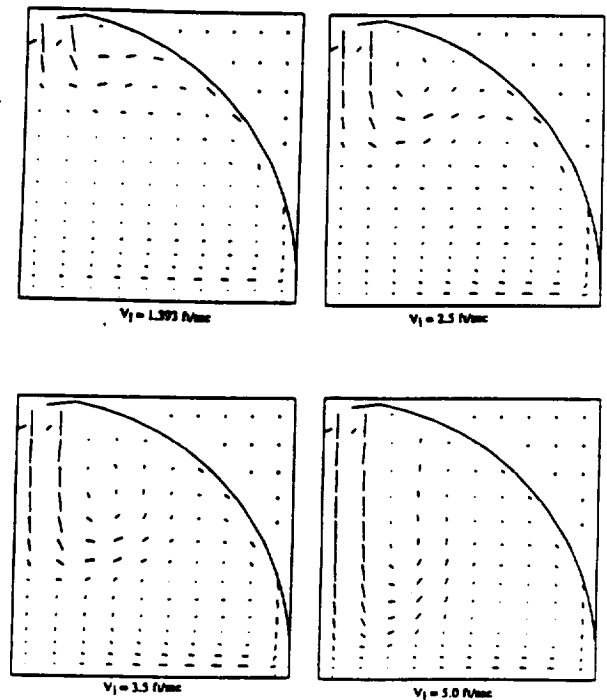


Figure 15 End of pressurization velocity fields (slush)

differences due to changes in heat flux rates and depending on whether slush or liquid hydrogen is being pressurized. As already noted, the hot pressurant gas penetrates the ullage more deeply when pressurizing slush than when pressurizing liquid hydrogen.

The final task undertaken during this study was to examine the predicted pressure history using the

dimensionless pressure, $P^* = \frac{(p - p_i)}{(p_f - p_i)}$, and

dimensionless time, $T^* = \frac{t}{t_f}$, developed during the

previous study⁴. Figure 16 displays the pressure history predicted using the SLURP-generated constant boundary heat flux rates, Fig. 17 displays the history predicted using the adiabatic tank wall boundary, and Fig. 18 displays the history predicted using the obstacle heat storage model. When overlaid, these curves are close enough to be considered the same. Therefore, the pressure history when plotted using the dimensionless parameters is not significantly influenced by any of the parameters examined during the present study.

SUMMARY AND CONCLUSIONS

A multi-dimensional computational model of the pressurization process in liquid/slush hydrogen tanks was developed using the FLOW-3D computer code. In contrast with previously published multi-dimensional models, the heat flux rates from the ullage to the tank wall and to the liquid/slush are computed by the model rather than requiring a priori specification. The tank wall is modeled using a lumped heat storage model applied to azimuthal strips of the wall and the heat flux rates are computed from standard correlations.

The new model was used to study the influence of ullage boundary heat flux rates on the pressurization process. Analyses of both liquid hydrogen and slush hydrogen pressurization were performed to expose differences between the two processes. Predictions from the new model were compared to previously published predictions which used constant heat flux rates predicted by a one-dimensional model and to analyses based on an adiabatic interface between the ullage and the tank wall. For each of these models, analyses were performed over a range of pressurant mass flow rates. The pressurization predictions from these analyses are summarized in graphical displays to establish the functional interdependence between the parameters.

It is demonstrated that the ullage boundary heat flux rates do significantly effect the pressurization process. The pressurant mass requirement is shown to increase with increasing heat transfer rates at the ullage boundaries and to also increase with decreasing mass flow rate. It is shown that the entering pressurant gas more deeply penetrates the ullage when pressurizing liquid and

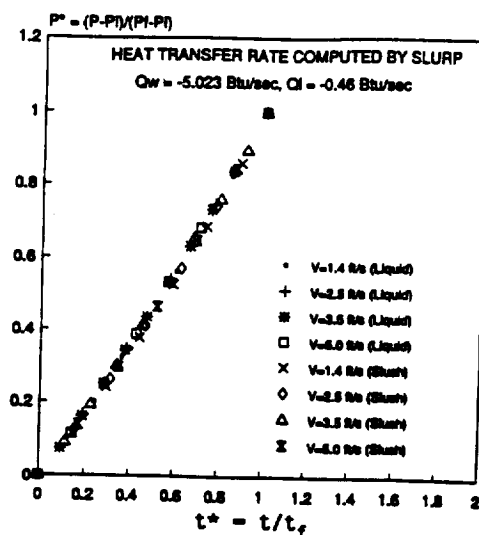


Figure 16 Dimensionless pressure history using ullage boundary heat flux rates from SLURP

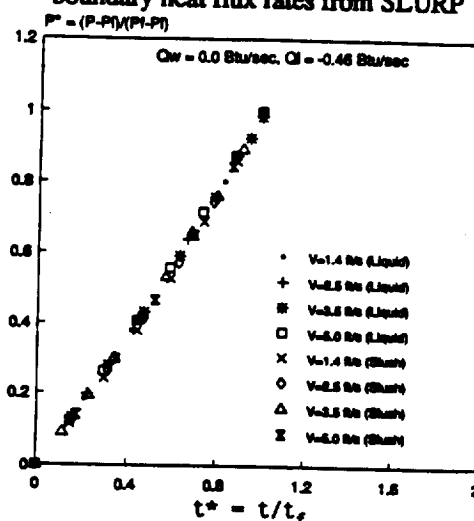


Figure 17 Dimensionless pressure history using ullage adiabatic interface at tank wall

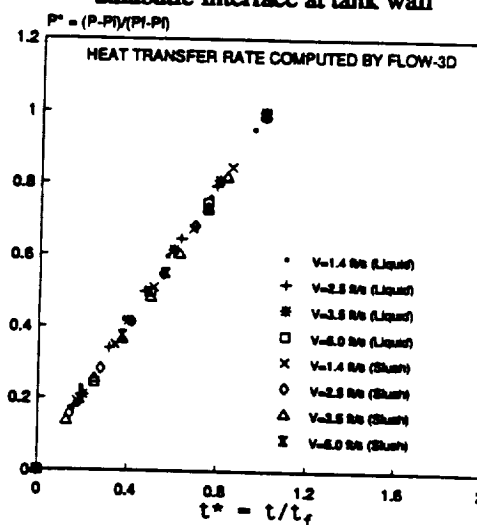


Figure 18 Dimensionless pressure history using correlations with obstacle heat storage model

that this results in a significant change in the temperature distribution in the ullage and the tank wall. The heat transfer rate from the ullage to the tank wall is shown to increase during the pressurization process and with increasing mass flow rate. Detailed velocity fields and temperature distributions are presented for selected cases to further illuminate the details of the pressurization process. Previously defined dimensionless pressure and time parameters are used to organize all of the pressure history profiles generated during this study. It is demonstrated that proper dimensionless scaling of pressure and time permit all the pressure histories examined to be displayed as a single curve.

REFERENCES

1. Hardy, T. L., and Tomsik, T. M., "SLURP: A computer code for Pressurization of a Slush Hydrogen tank Using Gaseous Hydrogen or Helium," NASP Technical Memorandum 1088, January, 1990.
2. Stochl, R. J., et al., "Gaseous-Hydrogen Requirements for the Discharge of Liquid Hydrogen from a 1.52-meter (5 ft)-Diameter Spherical Tank," NASA TN D-5336, August, 1969.
3. Stochl, R. J., et al., "Gaseous-Helium Requirements for the Discharge of Liquid Hydrogen from a 1.52-meter (5 ft)-Diameter Spherical Tank," NASA TN D-5336, January, 1970.
4. Sasmal, G. P., Hochstein, J. L., Wendl, M. C., Hardy, T. L., "Computational Modeling of the Pressurization Process in a NASP Vehicle Propellant Tank Experimental Simulation," 27th Joint Propulsion Conference, Sacramento, CA, June 1991.
5. "FLOW-3D/88: Computational Modeling Power for Scientists and Engineers", Flow Science, Inc., Los Alamos, New Mexico.
6. Hardy, T. L., Personal Communications, June 1991.